*32nd EPS Conference on Plasma Phys. Tarragona, 27 June - 1 July 2005 ECA Vol.**29C**, P-4.015 (2005)*

Comprehensive Measurements and Modeling of SOL, and Core Plasma Fueling and Carbon Sources in DIII-D

M. Groth,[1] G.D. Porter,[1] B.D. Bray,[2] N.H. Brooks,[2] M.E. Fenstermacher,[1] R.J. Groebner,[2] C.J. Lasnier,[1] W.M. Meyer,[1] M.E. Rensink,[1] D.L. Rudakov,[3] J.G. Watkins,[4] and L. Zeng[5]

[1]*Lawrence Livermore National Laboratory, Livermore, California, USA*
[2]*General Atomics, San Diego, California, USA*
[3]*University of California, San Diego, California, USA*
[4]*Sandia National Laboratory, Albuquerque, California, USA*
[5]*University of California, Los Angeles, California, USA*

Plasma boundary modeling of low density, low confinement plasmas in DIII-D has been benchmarked against a comprehensive set of measurements and indicates that recycling of deuterium ions at the divertor targets, and chemical sputtering at the divertor target plates and walls, can explain the poloidal core fueling profile and core carbon density. Key measurements included the 2-D intensity distribution of deuterium neutral and low-charge state carbon emission in the divertor and around the midplane of the high-field scrape-off layer (SOL). Chemical sputtering plays an important role in producing carbon at the divertor targets and walls, and was found to be a prerequisite to reproduce the measured emission distribution.

1. Introduction and Principal Diagnostics

Understanding the location and transport of hydrogenic fuel and impurity sources in present experiments is crucial for predicting the core plasma performance in future fusion devices. Pedestal models also indicate that the location of fuel ion recycling and neutral attenuation across the SOL and pedestal impact the plasma performance [1]. This paper focuses on the comparison of experimental data from well-diagnosed experiments in DIII-D to numerical simulations, to (a) validate the physics models used, and (b) to quantify impurity wall sources and the poloidal core plasma fueling profile.

Numerical plasma solutions were obtained using the edge fluid code UEDGE [2] and Monte-Carlo neutral transport code DEGAS2 [3], and validated against a large set of experimental data from edge diagnostics (Fig. 1), including the 2-D poloidal distributions of D_α, D_γ, CI (910 nm), CII (514 nm), and CIII (465 nm) in the divertor and main SOL (inner midplane) inferred from tangentially viewing cameras [4,5]. Other diagnostics utilized in this study are shown in Fig. 1. Neutral transport and core plasma fueling, as well as impurity sources and transport were extracted from the code simulations. In this paper detailed comparisons of the experimental results with the transport models are presented for a low density, low-confinement (L-mode) plasma in a lower single null magnetic configuration.

2. Experimental Measurements

In this work the analysis of DIII-D plasmas focuses on low-density L-mode discharges in a lower single-null configuration with the ion $\mathbf{B}\times\nabla B$ drift direction toward the lower divertor (Fig. 1). The first magnetic flux surface limited by the main wall was at the axisymmetric upper baffle limiter, 6.5 cm radially outward from the separatrix (outer midplane equivalent). The core plasma density was 2.6×10^{19} m^{-3}, or 23% the Greenwald density [6]. By sweeping of the

inner and outer strike points (ISP and OSP, respectively), radial profiles of the electron density and electron temperature from Langmuir probes (LPs) embedded in the target tiles, and of the deuterium and carbon emission from the lower vertical photomultiplier (PMT) array and spectrometer lines-of-sight were obtained.

The intensity distributions of deuterium neutral and carbon neutral and ion emission in the lower divertor is consistent with the assumption that, at this density, the outer divertor plasma was attached, while the inner leg was partially detached from the target plates. The D_α [Fig. 2(a)] and D_γ emissions in the divertor strongly peaked (by nearly two orders of magnitude) at the interface of the inner, 45 deg. slanted target plate with the center post. The neutral carbon emission distribution [Fig. 2(b)] also peaked (by approximately a factor 2 compared to the emission near the OSP) at the same location. Singly and doubly ionized carbon [Fig. 2(c)] was observed in the inner SOL near the divertor X-point and at the OSP region.

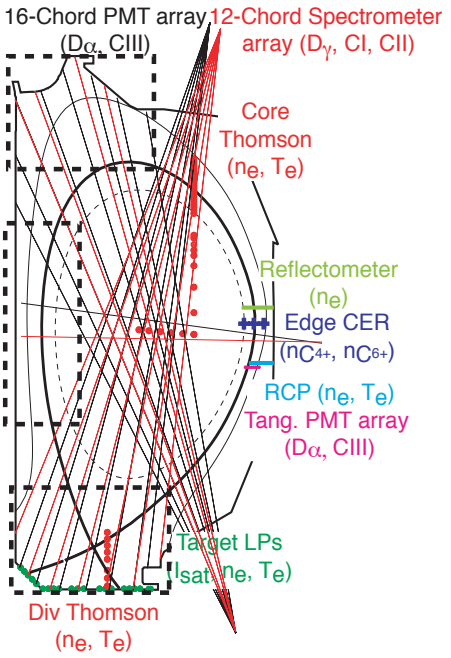

Fig. 1. DIII-D edge diagnostic system. The rectangles indicate the fields-of-view of the tangential cameras. Also shown is the magnetic configuration of DIII-D discharges 119919 at 3 s (reference discharge).

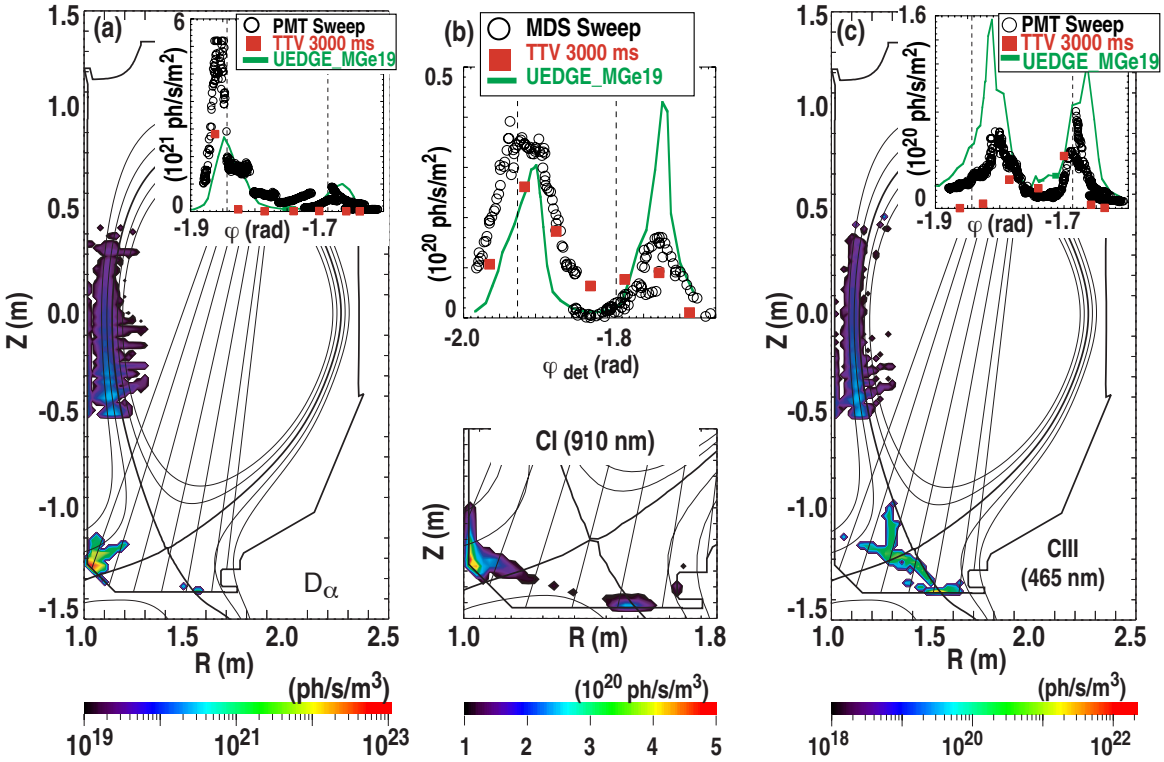

Fig. 2. Reconstructed D_α (a), CI (910 nm, b), and CIII (465 nm, c) intensity distribution from image data of the lower and high field, midplane SOL. The inserts show the poloidal profile of the emissions at the same wavelength obtained by the vertically viewing PMT and spectrometer arrays during the strike point sweep, compared to the same line-integrals across the reconstructed images, and the UEDGE/DEGAS2 plasmas solution. In the inserts the dashed lines indicate the location of the separatrix at the inner and outer target.

The electron temperature of the plasma nearest to the OSP was 12 eV and 25 eV, measured by divertor Thomson and LPs, respectively. At the inner target plate, the LPs indicated electron temperatures of 5 eV or less.

In the region of the high-field SOL, between –0.5 m below and 0.5 m above the tokamak equatorial plane, the D_α [Fig. 2(a),] CII, and CIII [Fig. 2(c)] intensity distributions peaked in the direction of the lower divertor X-point, suggesting that the particle sources were located in the divertor region. Between the ISP region and the peak of the high-field midplane SOL, the D_α emissivity decreased by more than two orders of magnitude, while the drop in CII and CIII emission near the inner X-point region to the inner midplane was of the order 10-50. From the region around Z = –0.5 m towards the midplane, the poloidal decrease of the emissions was nearly exponential along the flux surfaces; their fall-off lengths were 0.5 m (D_α), 0.3 m (CII), and 0.4 m (CIII).

The reconstructed 2-D emission profiles in the lower divertor and inner midplane SOL are consistent (within a factor of 2) with line-of-sight measurements from the vertical and horizontal PMT and multi-chord spectrometer [Fig. 2(a-c)]. In the absence of an absolute calibration, the latter was used to cross-calibrate the camera inversions for the D_γ and CI measurements.

3. Poloidal Core Fueling Profiles and Carbon Transport Using UEDGE/DEGAS2

Simulations of the described L-mode plasma using the UEDGE and DEGAS2 codes were validated against the set of diagnostics illustrated above, including the measured 2-D intensity distribution of deuterium and carbon emission in the divertor and main SOL. The calculated plasma solutions are consistent with most of the experimental data within a factor of 2-3 [Fig. 2(a-c)], a factor that also represents the uncertainty of some of the measurements and their shot-to-shot variations. Core plasma fueling, carbon sources, and carbon transport from the wall source to the core plasma ($\psi_N \sim 0.94$) were extracted from the codes. Here, DEGAS2 was run on a background plasma provided by UEDGE, and an added halo plasma region between the UEDGE numerical domain and the DIII-D walls. Constant electron densities and temperatures of 10^{17}–10^{18} m^{-3} and 2-4 eV were assigned ad-hoc to this region, consistent with the measurements by the outer midplane reciprocating probe and edge reflectometry.

The poloidal distribution of the neutral flux across the separatrix calculated by DEGAS2 shows that neutrals predominantly fuel the core from the high-field side in the vicinity of the divertor X-point up to 1m poloidally upstream. DEGAS2 neutrals were launched from the target plates only, with a poloidal distribution corresponding to the UEDGE calculated ion flux to the targets. Neutrals can reach the upstream SOL region by means of charge-exchange with plasma ions and reflections off the wall. The magnitude of neutral leakage in the DEGAS2 simulation is consistent to within a factor 2-5 with measurements of the D_α emission in the outer and inner midplane SOL, as well as with the neutral pressure ($\sim 2\times10^{-4}$ Pa) at the outer midplane.

The UEDGE simulations reproduced the measured neutral and low-charge state carbon emission in the lower divertor and around the inner midplane, indicating that chemical sputtering from the divertor targets and walls [7] provide a sufficient source to explain the upstream carbon density. In the simulations carbon was also produced at surfaces directly adjacent to the target plates,. Chemical sputtering from the main chamber surface plays only a minor role since ion and neutral fluxes to those surfaces are orders of magnitude lower than to the divertor. Reducing the chemical sputtering rates as suggested by Ref. [8] raises the OSP electron

temperature from 2-3 eV to 10-12 eV, more consistent with the measurement by divertor Thomson, but those plasma solutions did not reproduce the radiated power, its 2-D distribution, and the distribution of the low charge state carbon emission. The low physical sputtering rate in the OSP region is due to the lower plasma temperature obtained in the simulations.

Impurity **E×B** drifts and drag on fuel ions play an important role in the carbon transport dynamics, with carbon is preferentially transported from the outer to the inner divertor region. Consistent with measurements by Ref. [9], the simulations predict that carbon is swept from the private flux region to the inner divertor due to **E×B** drifts caused by the radial electric field near the separatrix. Flow reversal in the SOL region away from the separatrix allows carbon to drift upstream due to dominant ∇T_i forces, while in the region near the separatrix carbon is swept towards the target plate by drag from the background plasma flow. In the high-field SOL, the UEDGE simulations calculate poloidal fall-off lengths that are typically a factor of two longer than measured, indicating the existence of either stronger temperature gradients or lower background flows in the simulations than in the experiment.

By choosing a more realistic core boundary condition for carbon in UEDGE, the fully stripped and helium-like carbon densities as measured by charge exchange spectroscopy were well-matched with the code (factor of 2 and better), but those changes had very little effect on the lower charge state carbon distribution in the SOL. For the revised core boundary condition in UEDGE, a constant, radially outward flux of fully stripped carbon at the code core boundary, set equal to the sum of the lower charge state going inward across the same flux surface. The simulated CIII emission at the outer midplane shows agreement with the measured profile near the separatrix, but overestimates the emission further outboard by an order of magnitude.

Variations to uncertain input parameters, such as the target plate chemical sputtering yield, and boundary conditions, show how sensitive the plasma solutions are to those assumptions. Overall, the presented modeling cases indicate that recycling at the target plates, concomitant production of carbon at the plates, and ion leakage into the main SOL are sufficient to describe the data. Our progress in understanding carbon sources and transport is tightly linked to how well those assumptions can be validated from experiments.

This work was supported by the U.S. Department of Energy under W-7405-ENG-48, DE-FC02-04ER54698, DE-FG02-04ER54758, DE-AC04-94AL85000, and DE-FG03-01ER54615. The authors would like to thank J.A. Boedo, S. Brezinsek, E.M. Hollmann, T.W. Petrie, G. Wang, and W.P. West for their assistance with the experiments, and M.R. Wade and M. O'Mullane for their help with the analysis of charge exchange spectroscopy data.

[1] M.A. Mahdavi, *et al.,* Phys. Plasmas **10**, 3984 (2003).
[2] T.D. Rognlien, *et al.,* J. Nucl. Mater. **196-198**, 347 (1992).
[3] D.P. Stotler, *et al.*, Contrib. Plasma Phys. **34**, 392 (1994).
[4] M.E. Fenstermacher, *et al.,* Rev. Sci. Instrum. **70**, 974 (1997).
[5] M. Groth, *et al.,* Rev. Sci. Instrum. **74**, 2064 (2003).
[6] M. Greenwald, *et al.*, Nucl. Fusion **28**, 2199 (1988).
[7] J.W. Davis, *et al.*, J. Nucl. Mater. **241-243**, 37 (1997).
[8] D.G. Whyte, *et al.*, J. Nucl. Mater. **290-293**, 356 (2001).
[9] J.A. Boedo, *et al.*, Phys. Plasmas **7**, 1075 (2000).